XINGHUA LI, RUITAO FENG, XIAOBIN GUAN, HUANFENG SHEN, AND LIANGPEI ZHANG

Remote Sensing Image Mosaicking

Achievements and challenges

©ISTOCKPHOTO.COM/NLSHOP

In the past decades, remote sensing image mosaicking has attracted considerable attention in the community, and a large number of algorithms for remote sensing image mosaicking have been proposed. In the meantime, there are still several issues to be resolved. In this article, we review state-of-the-art remote sensing image mosaicking methods focused mainly on aspects of radiometric normalization, seamline detection, and image blending. We also analyze the achievements and challenges of remote sensing image mosaicking.

Image mosaicking is often a necessary process to cover a large and full region of interest (ROI) for many remote sensing applications (e.g., geographical mapping, resource and environmental monitoring, and disaster monitoring).

Digital Object Identifier 10.1109/MGRS.2019.2921780
Date of current version: 18 December 2019

BACKGROUND

Due to the limitations of the imaging width or mechanism, it is common that the ROI cannot be contained in only one remote sensing image scene. For a sensor on a remote sensing platform to obtain higher resolution, the captured scene must become narrower. Accordingly, it is often necessary to mosaic multiple images to capture the full ROI or a wide field-of-view (FOV) scene [1]. In fact, image mosaicking is the process of merging two or more images with overlapping areas into a single view having an indistinguishable seamline [2]. Among the main purposes of image mosaicking are illustrative use, information extraction, and geographical mapping. Therefore, prior to many practical applications, image mosaicking is often an essential task in remote sensing image processing [3], [4], resource and environmental monitoring [5], [6], and so on.

For example, NASA sponsored the creation of the Tri-Decadal Global Landsat Orthorectified data collection by mosaicking Landsat Multispectral Scanner (MSS), Thematic Mapper (TM), and Enhanced Thematic Mapper Plus (ETM+) images. The data set was generated from approximately 7,550 MSS (*Landsat 1–3*) images, 7,413 TM (*Landsat 4–5*) images, and 8,500 ETM+ (*Landsat 7*) images [7]. There are also many other large-scale remote sensing

image mosaics, such as the Advanced Very High Resolution Radiometer mosaic of the Antarctic continent produced by the National Oceanic and Atmospheric Administration, the United States Geological Survey, and the British National Remote Sensing Center in 1985 [8]; the Global Rain Forest Mapping (GRFM) project over the tropical belt led by the National Space Development Agency of Japan [9], [10]; and the Central Africa Mosaic Project carried out by the European Space Agency and the German Aerospace Center [5].

Image mosaicking has gone through a long period of development, and a large number of algorithms has been proposed. Generally speaking, image mosaicking consists of five aspects: image registration [11], extraction of overlapping areas, radiometric normalization [12], [13], seamline detection [14], [15], and image blending [16] (see Figure 1). A successful mosaic usually has an underlying requirement that the multiple images to be mosaicked have a consistent geometry [7], which is ensured by image matching or image registration. After the images are aligned, the extraction of overlapping areas provides the foundation for the subsequent radiometric normalization, seamline detection, and image blending. Relatively speaking, it is very simple to extract the overlapping areas. On the one hand, for remote sensing images without geographic reference information, the overlapping areas can be extracted by phase correlation [17] or scale-invariant feature transform (SIFT) [18]. On the other hand, for remote sensing images with geographic reference information, georeferencing information can be used for the extraction of the overlapping areas. Georeferencing information can be either the geographical coordinates of the images (e.g., GPS data) or onboard position and attitude data (e.g., inertial navigation system data) [19], [20]. To ensure a satisfactory mosaic result, intensity balancing should be undertaken to make the intensities of the images as consistent as possible. Seamline detection involves finding the optimal seamline locations among the images. Based on the detected seamline, image blending reduces the differences along the seamline and merges the images to an integral individual.

Previous efforts in remote sensing image mosaicking have focused mainly on these five aspects. As far as we know, the state of the art of this field has not been summarized. Our intention in this review is to allow a better understanding of the achievements in image mosaicking and to overcome the challenges for future research. Image registration has been outlined by Zitová and Flusser [21], Dawn et al. [22], Bisht et al. [23], and Dalmiya and Dharun. Furthermore, the extraction of overlapping areas can usually be completed by simple methods. Therefore, we do not go into details on image registration and the extraction of overlapping areas. Instead, our attention is focused on radiometric normalization, seamline detection, and image blending. In this review, a number of methods of digital image mosaicking are also considered with regard to the universality of remote sensing image mosaicking.

RADIOMETRIC NORMALIZATION

To make the mosaicked image a single natural scene, radiometric normalization plays an important role. When the images taken from the same sensor at the same time are visually similar, their mosaic image looks like a very normal integral object. When the mosaic image is used as the geographical map, radiometric normalization, in particular, is not required. However, in most cases, radiometric normalization is necessary because the images to be mosaicked differ significantly in terms of radiation. In the literature, radiometric normalization is also called *radiometric balancing*, *tonal adjustment*, or *tonal correction*. Radiometric normalization is based on the premise that the reflection conditions in the overlapping areas remain constant [25]. Therefore, the corresponding pixel pairs in the same location from two different scenes are used to calculate the mapping relationship. In other words, the mapping relationship of radiometric normalization is derived from the overlapping areas and is then applied to the whole image (see Figure 2). For radiometric normalization,

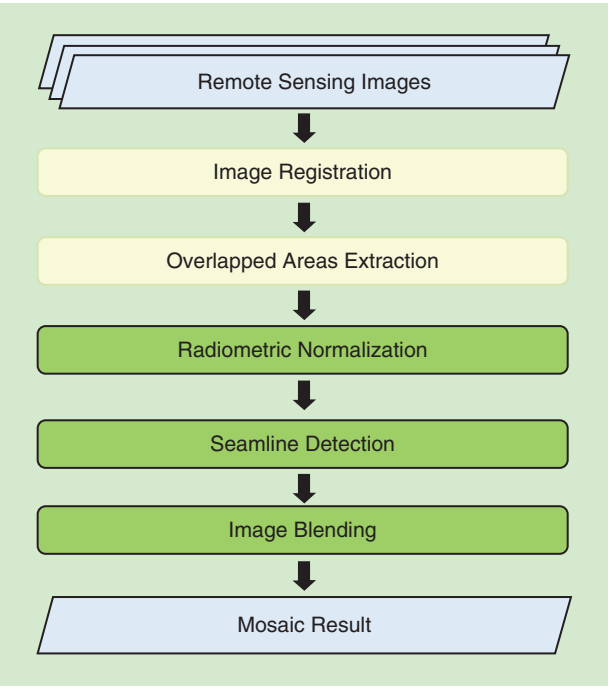

FIGURE 1. The procedure of remote sensing image mosaicking.

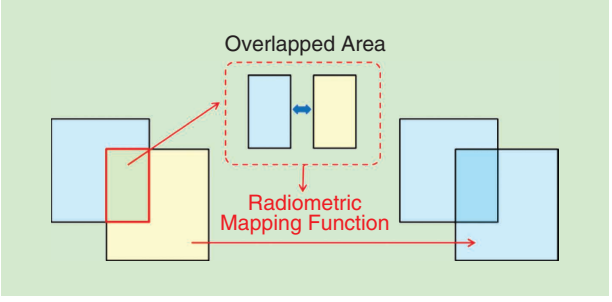

FIGURE 2. Radiometric normalization.

Cresson and Saint-Geours [26] proposed a global harmonization method by solving a quadratic programming optimization problem. This method can implement multiple remote sensing images simultaneously without any given reference image. However, the methods introduced in the following are usually based on a reference image. The main methods of radiometric normalization can be classified into global models, local models, and combined models.

GLOBAL MODELS

Global-model-based methods assume that the radiometric mapping relationship between the source and target images can be represented by a global linear or nonlinear transform, as shown in (1) [27]. The source image is the image selected as a reference, and the target image is the image whose intensity is to be corrected. The overall radiometric consistency is ensured by the following global model:

$$I_1^* = f(I_1), \tag{1}$$

where I_1 is the target image, I_1^* is the corrected target image, and $f(\cdot)$ is a linear or nonlinear function denoting the mapping relationships of all of the bands. Global-model-based methods can be further grouped into pixel-to-pixel and region-to-region methods.

PIXEL-TO-PIXEL METHODS

Pixel-to-pixel methods directly model the radiometric mapping relationship using the intensity values of the corresponding pixel pairs. When the objects in the overlapping areas are not changed or the images are captured very closely in time, the relationship of the pixel pairs can be regarded as linear. In this situation, linear regression [25], [28] and least-mean-square (LMS)-based transformation [29], [30] for all of the pixel pairs are two effective approaches. In addition, Chen et al. [31] proposed a method based on iteratively reweighted, multivariate alteration detection transformation and orthogonal regression [32] to reduce the error of radiometric normalization: they achieved radiometric consistency by considering the effect of the normalization path on the normalization coefficients.

Usually, all pixels in the overlapping areas are used to build the relationship. However, not all pixels always satisfy the linear assumption. Thus, the characteristic pixels that meet the linear assumption in the overlapping areas need to be carefully selected. For example, Yong et al. [33] applied band-specific principal component analysis to select the characteristic pixels. Zhang and Georganas [34] selected the principal regions using an intensity histogram to construct the transform matrix based on the average intensity values. This method is very fast, but it is not known how the accuracy of the registration affects the radiometric normalization. Radiometric inconsistency can also be corrected according to the imaging mechanism. Litvinov and Schechner [35] corrected radiometric mismatch by estimating the radiometric response and camera nonuniformity simultaneously, based on a computer-vision tool and the physical process of the imaging system. The results they obtained were very satisfactory, indicating that mosaicking can be successfully achieved without resorting to any type of feathering method.

Pixel-to-pixel methods utilize the mapping relationship directly derived from the pixel pairs to correct the radiometric differences. These are the basic methods of radiometric normalization, and they usually obtain satisfactory results for consistent radiometric differences. However, in most cases, they are very sensitive to the accuracy of the image registration. These methods can thus achieve a good effect when registration accuracy is high and radiometric difference is consistent.

REGION-TO-REGION METHODS

The region-to-region methods utilize the statistical information (e.g., mean, standard deviation, and variance) of the intensity in the overlapping areas to construct the radiometric mapping function [36]. Compared with pixel-to-pixel methods, region-to-region methods indirectly model the mapping relationship from pixel pairs. An advantage of this method is that the pixel pairs are not required to be strictly aligned. When the objects in the overlapping areas are changed, especially for multitemporal remote sensing images, region-to-region methods are more effective than pixel-to-pixel methods. The representative methods include diagonal-matrix transformation models [37], [38], histogram matching [39]–[42], moment matching [43], [44], Wallis transformation [45], and quadratic programming color balancing [26].

Among region-to-region methods, the diagonal-matrix transformation models are very basic and simple, and they use the mean intensity of the neighboring images to calculate the relationship. For example, Tian et al. [37] proposed a six-parameter diagonal model to compensate for the radiometric differences by spectral transformation between images. In their view, the basis of this approach is that the reflected light depends on the spectral properties and the illumination angle on the surface. Generally speaking, the diagonal models are suitable for remote sensing images with ordinary scenarios or a low spatial resolution.

The histogram-matching-based methods make the histogram in the overlapping areas of the target image similar to that of the source image. These methods assume that the radiometric mapping function has no particular parameters, and most of them apply a lookup table to directly record the mapping relationship of the source and target images [27]. Generally, the lookup table is constructed from the joint histogram of the image features or pixel pairs in the overlapping areas. Interestingly, Xie et al. [46] proposed global optimization to realize intensity consistency, guided by an initial solution of the histogram extreme-point matching strategy. Based on the histogram,

Jia et al. [47] generated an optimal radiometric mapping function between a poorly exposed image and a motion-blurred image by considering radiometric statistics and spatial constraints simultaneously. Kim and Pollefeys [48] estimated the brightness transfer function by dynamic programming (DP) with the intensity histogram in the overlapping areas. Yamamoto and Oi [49] used a joint histogram of the SIFT feature between two neighboring images to estimate the radiometric mapping function. In summary, histogram-matching-based methods can acquire excellent global radiometric balancing using the intensity distribution information.

Moment matching, as depicted in (2), utilizes the mean and standard deviation of the overlapping areas to calculate the relation function. In the following, the mean value represents the average of the image intensity, and the standard deviation represents the variability of the image intensity, both of which are considered to be the basic indicators for image color:

$$I_1^* = I_1\left(\frac{\sigma_2}{\sigma_1}\right) + \mu_2 - \left(\frac{\sigma_2}{\sigma_1}\right)\mu_1, \tag{2}$$

where I_1 is the target image; I_1^* is the corrected result of I_1; σ_1 and σ_2 are the standard deviations of the overlapping areas in I_1 and the source image I_2, respectively; and μ_1 and μ_2 are the means of the overlapping areas in I_1 and I_2, respectively. The strategy of matching the mean and standard deviation also works well in a color space with decorrelated axes [50]. Moment matching can obtain a similar effect to the LMS-based methods when the images have a high registration accuracy. However, moment matching is much less sensitive than LMS-based methods to registration accuracy.

Wallis transformation is a similar approach to moment matching; it uses the mean and variance [51] in the overlapping areas to adjust the radiometric differences. This approach considers that the intensity variances describe the variability of the image radiometric intensity. In fact, when the standard deviation values in (2) are replaced by the corresponding variances, moment matching is converted into Wallis transformation. In most cases, Wallis transformation obtains a similar result to moment matching.

The previous four method types use the statistical properties from different angles and patterns to fulfill radiometric normalization. In summary, because the region-to-region methods model the radiometric mapping relationship according to the statistical information of the overlapping areas, they are not sensitive to registration accuracy. For radiometric differences with an overall consistency, the region-to-region methods can achieve a satisfactory effect.

LOCAL MODELS

As stated previously, global models are very effective for the correction of consistent global radiometric difference. However, they ignore, to some extent, local radiometric differences. When the image contents are complex or the images have a high spatial resolution, the transferred intensity from the overlapping areas to the full image will create local inconsistency with a global model. In other words, local differences will still exist in the images. As a result, local models have been put forward to consider local radiometric differences. Compared with global models, there has been less research into local models. The basic principle of the local model is to correct the local radiometric differences according to the regional features.

For example, Tai et al. [52] addressed the problem of local color transfer by probabilistic segmentation and regional mapping using the expectation-maximization algorithm and a Gaussian mixture model. However, this method can achieve a natural transition only across regions without complex scenes. To solve this problem, Xiang et al. [53] further improved this method when a set of source images is available. The probabilistic color-correction algorithm [54] computes a series of local color palette mapping functions by fitting a set of univariate truncated Gaussians to the observed color mappings. The local mapping functions are then used to correct the intensity differences of the different regions. Local moment matching [3] adjusts the intensity of the target image using different moment matching models in different regions. The effect of this approach is satisfactory, but the size of the local regions needs to be determined empirically. Li et al. [55] proposed a pairwise gamma correction model to coarsely align the intensity between the source and target images. The radiometric differences are then further reduced by the least-squares adjustment method.

At the core of the local models is designing suitable regional normalization functions according to the characteristics of local radiometric differences. Local models can effectively solve the local inconsistency of the intensity, and they are a valuable complement to the global models. However, local models can also bring about new radiometric inconsistency if the processing mode and level do not match with the local features. Therefore, it will be very valuable and interesting to design an adaptive local model.

THE COMBINED MODELS

Global models consider the overall consistency of the intensity, while local models take the local differences into consideration. In principle and effect, global and local models have complementary advantages. To integrate the respective advantages of the two types of models, a number of researchers have proposed combined global and local models. Usually, this is achieved by the global model's being first applied to reduce the global radiometric difference, and then the remaining local difference being corrected by the local model. To date, there has not been much research on combined models, and the main works are as follows.

Jia and Tang proposed an optimal mapping function for global and local intensity replacement by a modeless replacement function [56] and tensor voting [57], respectively. The radiometric alignment is achieved by the replacement

function propagating the curve smoothness constraint in a dense tensor field. Based on a global-to-local strategy, Pan et al. [58] developed a network-based radiometric equalization approach to eliminate the radiometric differences between images. The linear model is globally enforced on the images, and the nonlinear model is enforced in the overlaps to optimize the local performance. Similarly, Yu et al. [59] proposed a global-to-local radiometric normalization method that combines global and local optimization strategies to eliminate the radiometric differences between images adaptively without assigning the reference image. The global optimization strategy constraint is that the radiometric differences between the images before and after processing should be minimal and the local optimization strategy should eliminate the radiometric differences in the overlapping areas.

In summary, global models use one function to correct the radiometric difference, and local models adopt different local functions to balance the differences. Combined, the models provide an overall consideration of the global consistency and local difference of the radiometric normalization. Technically speaking, whichever model is selected for radiometric normalization, the radiometric mapping function is usually estimated from the overlapping areas of the target and source images and then extended to the nonoverlapping areas of the target image. By the use of this process, the visual artifacts should not be imported. With the improvement of the spatial resolution of remote sensing imagery, the combined models will provide a more promising direction in the future for radiometric normalization.

SEAMLINE DETECTION

Determining the optimal seamline location is a prerequisite for achieving a seamless mosaic. The optimal seamline is the location where the images share the most intensity and texture similarity. Duplaquet [60] listed the following requirements for an optimal seamline: 1) on the seamline, the intensity difference of pixels in the two images is minimal, and 2) the geometric difference along the seamline is minimal. However, it is not necessary to find the optimal seamline for all types of remote sensing images.

For low- or medium-resolution remote sensing images, the image information content and structure are simple: the initial seamline can be directly determined by the geometrically straight lines of the overlapping area (e.g., the diagonal and middle lines in Figure 3), which will be optimized subsequently. For high-resolution remote sensing images, because of the differences in projection, illumination, and moving objects, the optimal seamline should be identified [61]. It is preferable that the seamlines are curves [see Figure 3(c)] because straight lines are more easily detectable by the human eye [62]. According to the difference in the data sources, seamline detection methods include two categories: image-internal-information-based and external-data-based methods.

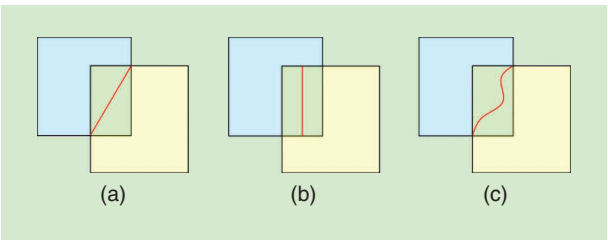

FIGURE 3. The seamlines (denoted in red): the (a) diagonal line, (b) middle line, and (c) curve.

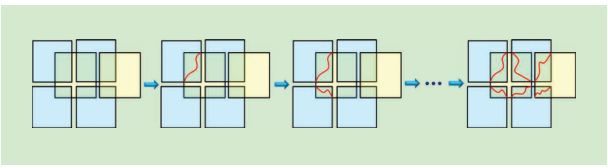

FIGURE 4. An example of frame-to-frame methods for seamline (denoted by the red lines) detection.

IMAGE-INTERNAL-INFORMATION-BASED METHODS

As the name implies, image internal information methods use only the information in the images to detect the optimal seamline. The intensity, texture, and structure of the images usually determine the path of the optimal seamline. This method type can be further categorized into frame-to-frame and multiframe joint methods.

FRAME-TO-FRAME METHODS

Frame-to-frame methods use mainly geometric, intensity, and texture features of the images themselves to detect the seamlines for the overlapping areas in every pair of neighboring images. As shown in Figure 4, multiple seamlines are detected one after another by frame-to-frame methods. The main methods are the bottleneck model [62], the snake model [63], Dijkstra's algorithm [64], the DP algorithm [65], and graph-cut based methods [66].

The simplest and most-direct method of seamline detection is the bottleneck model. For this model [62], the cost function is defined by the intensity differences. The optimal seamline traverses as little as possible the area with the maximum differences. To cope with the large intensity differences in the overlapping areas, the bottleneck model has been refined by the greedy, randomized, adaptive search procedure [67]. However, the bottleneck model struggles to obtain an adequate effect in regions with complicated textures.

Another classical seamline detection method is the snake model. This model [63] aims at a spline, with minimal energy, constrained by external and image forces. A snake is an active contour that moves through an image and changes its shape until a minimum of its energy function is obtained, which can be an edge, a line, or a subjective contour. The energy function of a mismatching value is composed of the internal energy, photometric terms, and

external constraint forces. The line with minimal energy is the optimal seamline. However, a local minimum is often obtained by the snake algorithm. The improved snake model [68] was proposed to solve—although not completely—the local optimum of the photometric terms with the Bresenham algorithm by multiple circulation. The twin-snake model [69], [70] is an extension of the snake model; here, two snakes approach the line in the overlapping areas from the opposite borders and are forced to approach one another. The optimal seamline is the result of merging the two snakes. This approach comes with a high computational cost, and the twin-snake model also cannot overcome the local minima problem [71]. Because the snake model and twin-snake model add constraints other than the intensity difference, they can achieve a better result than the bottleneck model.

A large amount of effort has focused on the popular Dijkstra's algorithm [64], which is widely used to find the shortest path. Based on this method, many seamline detection methods have been proposed. The seamline is the path that has the lowest cost from one edge of the overlapping areas to the other. For example, Davis [72] used this method to detect the optimal seamline of an image with moving objects. The relative difference between the two neighboring images measures the similarity of the overlapping areas. In addition, Dijkstra's algorithm was optimized in a weighted graph by the authors of [73] and based on image segmentation [74]. To avoid the complete obstacle area, the semiglobal-matching-based method [75] has been used to guide Dijkstra's algorithm to find the seamline. Pan et al. [76] proposed the two-level (pixel-level and object-level) seamline optimization approach based on the region change rate, in which the pixel level is based on Dijkstra's algorithm. Similarly, Wang et al. [77] extracted the seamline with marker-based watershed segmentation [78] at the pixel and the object levels. Dijkstra's algorithm is very robust for seamline detection. Therefore, with a predesigned path, researchers commonly resort to it for selecting the least-cost seamline.

In fact, Dijkstra's algorithm is also a type of DP algorithm [65] that is extensively used in seamline detection. Firstly, Duplaquet [60] developed a DP algorithm to search for an invisible seamline with a higher efficiency than Dijkstra's algorithm. Wen and Zhou [79] then combined DP and gray relational analysis to detect the best seamline. Chon et al. [80] found a longer seamline with fewer highly mismatched pairs by a cost conversion. In addition, the DP algorithm was refined by improved criteria and improved templates with an eight-direction Sobel operator by [81]. To avoid the seamline's going through buildings, Li et al. [3] proposed an automatic piecewise DP (APDP) method with five search directions (see Figure 5). The piecewise detection controls the deviation of the optimal seamline so that it can avoid ghosting. The DP algorithm provides a flexible framework for seamline detection by weighting different constraints. With an appropriate modification according to the image features, it is very robust and effective for remote sensing images.

Graph-cut-based methods are another practical way to detect the optimal seamline [66]. The basic idea is to construct a specialized graph representing the energy function such that the minimum cut on the graph also minimizes the energy [82], [83]. Kwatra et al. [84] utilized the graph-cut technique to determine the optimal patch region for any given offset from the input image and output image. Agarwala et al. [85] combined a set of photographs into a single composite image by graph cuts to optimize the seamline, and then they used gradient fusion to reduce the visible artifacts. Gracias et al. [82] further used watershed segmentation and graph cuts to find the best seamline. To avoid moving objects, Qu et al. [86] applied the min-cut/max-flow algorithm to search for the optimal stitching line. Graph-cut-based methods can be computed very efficiently by penalizing the radiometric difference.

Additionally, other methods have been proposed based on geometric, intensity, and texture features. For example, Levin et al. [87] and Zomet et al. [88] detected the seamline in the gradient domain to reduce seam artifacts and edge duplication. A bisector seamline algorithm proposed by Yang et al. [89] is based on the geometric characteristics in the valid overlapping areas of the remote sensing images. A seam planning algorithm [90] has also been applied to utilize the cost function of the path planning and so detect the seamline. To constrain the seamline along a road, a method based on edge detection was put forward recently by Nguyen et al. [91]. Laaroussi et al. [92] used the histogram-equalization-based method to find the optimal seamline to avoid dynamic objects in the images. All the used features aim at restraining the seamline along radiometrically equal regions so that the optimal seamline can be invisible.

MULTIFRAME JOINT METHODS

Frame-to-frame methods are usually effective for a small number of images. Once the seamline of a pair of images is detected, the same method can be applied to the other pairs of images, as in [93]. However, for a large data set, this approach has low efficiency as it is dependent on the

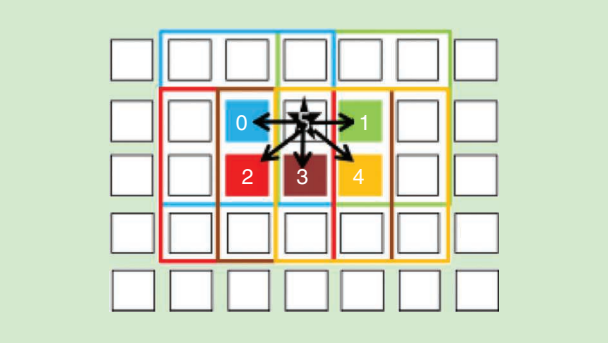

FIGURE 5. The five search directions for a seamline in an APDP [3].

composite sequence and the requirement for intermediate treatment. In contrast, multiframe joint methods are more efficient, as shown in Figure 6. These methods can simultaneously compute a seamline network for multiple images. In other words, the seamlines for all of the images are detected at the same time. The multiframe joint methods were developed on the basis of frame-to-frame methods in recent years, so they have on advantages in quantity.

Several methods have been developed for generating the seamline network based on a Voronoi diagram, as shown in Figure 7. Hsu et al. [94] first proposed a local-to-global method using ordinary Voronoi diagrams to generate a network of seamlines. However, it cannot be ensured that the seamline always lies in the overlapping areas. More effectively, based on area Voronoi diagrams with overlap (AVDO), a seamline network was formed automatically and effectively by Pan et al. [95]. This network is globally generated and can be further refined by the radiometric difference in the overlapping areas. Pan et al. [96] further improved the AVDO algorithm by including the detection of valid regions, providing a more general algorithm for generating bisectors, and refining the seamline network by combining the bottleneck model and Dijkstra's algorithm. Owing to the watershed segmentation algorithm, the bounded Voronoi diagrams [97] for a global seamline network generation are improved. The Voronoi diagram provides an excellent way for multiframe joint seamline detection. To obtain an outstanding seamline network that bypasses the integrated objects, preliminary results of the Voronoi-diagram-based methods should be further optimized.

The framework of graph cuts has also been introduced into the multiframe joint optimization strategy for seamline detection [98]. This method allows a simple human–computer interaction to constrain the image regions the seamlines will or will not pass through. Based on the optimal network vertices, the seamlines with the shortest paths between vertices can be detected by a graph-based approach [99]. Pan et al. [100] proposed an initial seamline network generation method based on improved seeded region growing, where the boundary of the overlapping areas is selected as the seed of the algorithm. This method is raster based and can address concave polygonal overlapping regions.

Compared with frame-to-frame methods, multiframe joint methods significantly increase the efficiency of seamline detection by omitting intermediate treatments. At the same time, the result is improved by the replacement of serial detection with global optimization. Based on only the information in the images themselves, multiframe joint methods can achieve a great effect. However, their efficiency can be further improved by introducing external data.

EXTERNAL-DATA-BASED METHODS

Traditional methods of seamline detection are based on only the images themselves. In recent years, methods based on external data have attracted increasing attention. These external data can guide the seamline to bypass ground objects (e.g., buildings), which brings a new concept to seamline detection. The main works are listed as follows.

First, lidar point clouds were used for seamline detection in [101]. Wang et al. [102] adopted a vector road map to generate seamlines; here, the vector road data are applied to construct a weighted graph, and Dijkstra's algorithm finds the lowest-cost path as the seamline. Similarly, Wan et al. [103] used vector road data to search for the seamline, but they instead applied the Floyd–Warshall algorithm [104] to find the lowest-cost path. A region-based saliency map [105] generated by a human attention model [106] has also been used to guide the seamline, which is also guided by pixel-based image similarity and location constraints. To avoid discontinuity in the mosaic, the information of ground object classification has been imported for seamline detection [107], where the object classes are obtained by the normalized difference vegetation index and the morphological building index.

A digital surface model (DSM) is commonly applied to detect seamlines. For example, Chen et al. [108] used the elevation information from a DSM to guide a seamline toward a low area by stereo matching. Based on the initial seamline network of the Voronoi diagram algorithm, Zheng et al. [109] and Zheng et al. [110] used the DSM to detect the edge diagram, which is finally refined by the weighted A* algorithm. To avoid buildings, on the one hand, a DSM can be applied using a gradient operator [111]; on the other, object heights can be derived from

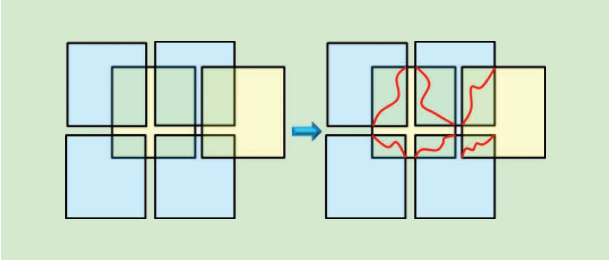

FIGURE 6. A multiframe joint method for seamline (denoted by the red lines) detection.

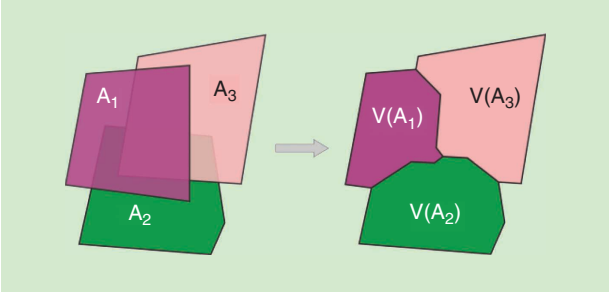

FIGURE 7. Seamlines based on a Voronoi diagram.

the DSM, and seamline detection can then be cast as a graph-cut problem [112]. With the help of external data, the optimal seamline can be detected with a weakened dependence on the image information itself. In brief, external data can provide favorable ancillary information for seamline detection.

Owing to the differences in radiation, illumination, projection, and so on, a reasonable way to obtain a seamless mosaic is to find an optimal seamline for a smooth transition from one image to another neighboring image. For the image internal information methods of seamline detection, frame-to-frame methods are less efficient than multiframe joint methods. Moreover, frame-to-frame methods usually bypass the obvious ground objects, while multiframe joint methods cannot. Thus, multiframe joint methods are often accompanied by certain optimization strategies.

IMAGE BLENDING

Minor radiometric inconsistency can still exist around the detected optimal seamline. To obtain a natural and smooth transition from one image to another neighboring image, image blending (also known as *seamline elimination*, *feathering*, or *alpha blending*) is usually required [87]. A large number of image-blending methods have been proposed.

Only a few methods have been suggested to get rid of differences directly. Peleg [113] removed the seamline by subtracting a smooth seam-eliminating function. Similarly, a hard correction method [114] can be used to compute the average gray difference between the pixels along the seamline and then adjust the gray difference to the pixels [89]. To some degree, hard correction is similar to the linear transition method [115], [116] and Poisson image editing [117], [118]. Whitaker [16] proposed a level-set blending method by minimizing the difference metric on the level set rather than the differences in pixel intensity values. The differences along the seamlines can also be reduced by a low-frequency smoothing approach [8] or the use of a median filter operation [45]. Generally speaking, direct elimination along the seamline can reduce the radiometric differences effectively but not completely.

To reduce the artifacts along a seamline, a weighted combination of the two neighboring images within a transition zone is commonly used. This combination can be achieved by the use of a bilinear weighting function [17], weighted averaging [12], [71], [87], [119]–[121], or mean value seamless cloning [18]. In other words, each image is multiplied by a weighting function in the transition zone and then summed to form the final mosaic. The core of this method is the weighting function, which should decrease monotonically with the distance from the seamline. Typical weighting functions are inverse distance weighting (IDW) and inverse cosine distance weighting (ICDW) [3]. As shown in Figure 8, the yellow rectangular region is the overlapped area of images a and b. In a given buffer, d_i denotes the distance from point P_i of image b to the seamline. For a smooth transition between the buffer of the two images, this is often

$$P_i^f = \omega_i^a P_i^a + \omega_i^b P_i^b, \tag{3}$$

where P_i^a and P_i^b are the pixels in P_i from image a and image b, respectively; ω_i^a and ω_i^b ($\omega_i^a + \omega_i^b = 1$) are their corresponding weights; and P_i^f is the final mosaic result. The weights are usually a function of the distance. As shown in Figure 9, ICDW has a smoother effect in the edges (for 0 and 1) than IDW.

There are many types of weighting strategies. For multiresolution blending, the weighting strategy can be realized with a pyramid [1], [2], [122], [123]. In addition to the image domain, weighted blending is also suitable for the gradient

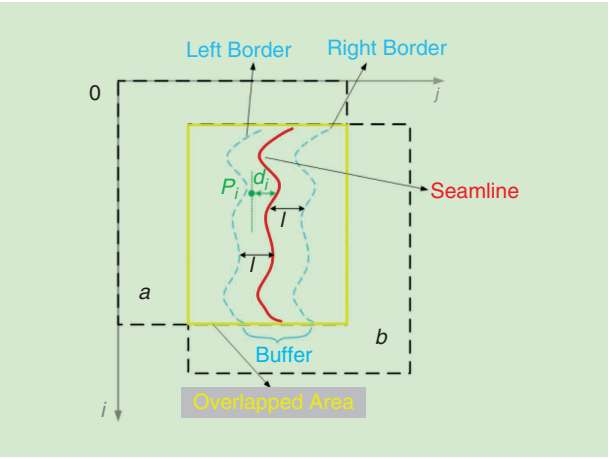

FIGURE 8. The buffer for image blending [3].

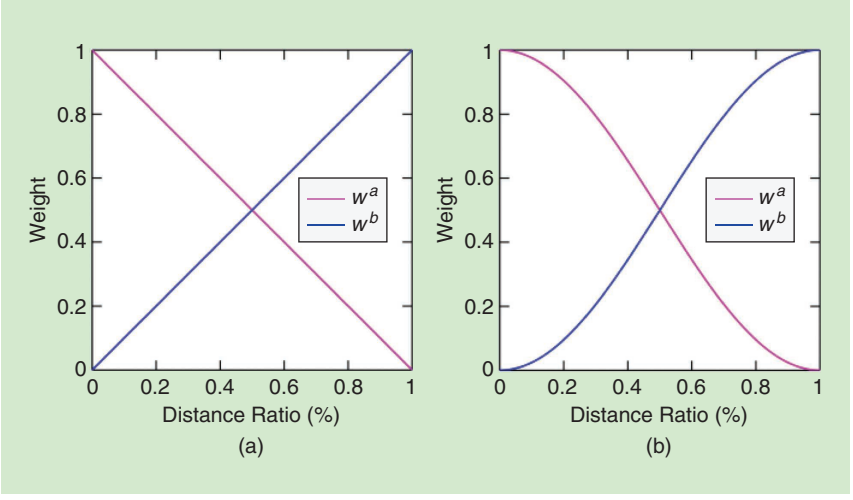

FIGURE 9. The weighting functions [3]: (a) IDW and (b) ICDW.

and the Fourier domains. For example, the gradient blending method [124] merges the images with a weighted combination according to a normalized lookup table. In the Fourier domain, the pixel averaging method [125] and weighted fusion [126] can be applied. Zhao [127] proposed a flexible image-blending method using a weighting function of the geometry, temporal order, and user control inputs, where the weighting functions are individually computed per frame.

IN THE PAST SEVERAL DECADES, REMOTE SENSING IMAGE MOSAICKING HAS UNDERGONE RAPID DEVELOPMENT, ESPECIALLY IN TERMS OF RADIOMETRIC NORMALIZATION, SEAMLINE DETECTION, AND IMAGE BLENDING.

The energy minimization strategy can also be applied in image blending. Su et al [128] proposed an energy minimization blending model in the wavelet space that balances the smoothness in the overlapping area and the fidelity of the original image. Wang and Ng [129] developed a variational blending method that uses the smoothness assumptions of the mask functions and boundary conditions in the overlapping areas. For temporally sequential images, an analytic minimization criterion [130] has been designed to optimize the blending coefficient by considering the temporal variations of the background, the temporal delay, and the image resolution. Relatively speaking, energy minimization methods are effective in eliminating the radiometric differences along the seamline. However, they usually have a higher computational cost than the weighting strategies.

As we know, image blending is affected by the result of the radiometric normalization and seamline detection. If the previously obtained radiometric normalization and seamline detection results are not satisfactory, it is difficult to obtain a natural transition effect with image blending. As a result, a great deal of effort is paid to radiometric normalization and seamline detection. Generally speaking, a weighted combination of images in the overlapping areas performs well. Nevertheless, the neighboring images should be precisely aligned; otherwise, the final result will contain ghosting.

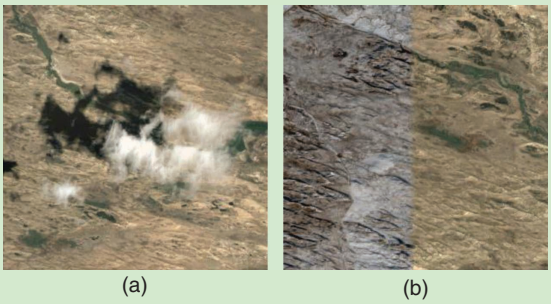

FIGURE 10. Two example images of Shari Yingaole, Abag Banner, Xilin Gol, China, cropped from Google Earth on 4 December 2018: (a) 43.328101° north, 115.54889° east and (b) 43.333141° north, 115.520999° east.

FUTURE DIRECTIONS

In the past several decades, remote sensing image mosaicking has undergone rapid development, especially in terms of radiometric normalization, seamline detection, and image blending. The efficiency and effectiveness of image mosaicking have been improved greatly. However, with the development of sensor technology and application requirements, remote sensing image mosaicking faces new opportunities and challenges. To the best of our knowledge, future directions for remote sensing image mosaicking include, but are not limited to, generalized, accelerated, integrated, and smart (GAINS) remote sensing image mosaicking.

GENERALIZED REMOTE SENSING IMAGE MOSAICKING

Usually, the goal of remote sensing image mosaicking is to obtain a full ROI or a wide FOV scene. In the future, the application and concepts of remote sensing image mosaicking should be generalized and extended. For example, image mosaicking will contribute to generating spatially continuous and high-quality remote sensing images. Optical remote sensing images are often subjected to cloud covers, so the images themselves include missing information [131]. As shown in Figure 10(a), the image cropped from Google Earth is contaminated by clouds. Assuming that the cloud-free image from another sensor or another time is available, the cloud in the current, cloud-contaminated image can be removed by the mosaic of the cloud-free and cloud-contaminated images [132]–[134]. In this sense, the cloud removal of remote sensing images is one type of generalized mosaicking. In other words, the goal of image mosaicking is not only to enlarge the scene range but also to improve the spatial continuity of the image. To obtain a spatially continuous image, multisource, heterogeneous images from different sensors may be involved in a generalized mosaic. The radiometric normalization of multisource heterogeneous images is very challenging, as shown in Figure 10(b). The concepts and applications of remote sensing image mosaicking will be not limited to expanding the scene: they will be generalized in the future.

ACCELERATED REMOTE SENSING IMAGE MOSAICKING

With the ongoing development of sensor technology, the spatial resolution of remote sensing image mosaicking becomes increasingly higher, and the data grow larger and larger. For remote sensing image mosaicking of a large-scale project, the data amount can be staggering. As we know, image mosaicking is both data and computation intensive. In the context of big data, traditional sequential computation techniques cannot meet the requirements of large-scale image mosaicking applications [135]. To achieve the requirements of real-time mosaicking,

high-performance computing such as parallel computing [31], [136], cloud computing [137], and distributed computing is considered a very promising direction. In addition, hardware systems (such as field-programmable gate arrays and graphics processing units) and hardware implementation methods (e.g., memory space conversion [138]) may also be effective ways to speed up the calculation process.

INTEGRATED REMOTE SENSING IMAGE MOSAICKING

As stated previously, image mosaicking usually consists of image registration, the extraction of overlapping areas, radiometric normalization, seamline detection, and image blending. Generally, the five steps are conducted sequentially and independently. To some degree, the independent processing strategy of image mosaicking restricts the automation of remote sensing image mosaicking. For a remote sensing image with high spatial resolution, the accuracy of image registration can hardly meet the demands of mosaicking. Therefore, high-spatial-resolution remote sensing images should be converted into orthorectified products before mosaicking. The operational production system of orthorectification usually needs high-accuracy auxiliary data (e.g., a DSM), which cannot be obtained freely and openly in most cases. This also reduces the efficiency and convenience of mosaicking. In the future, the procedure of image mosaicking should be integrated automatically, especially for high-spatial-resolution remote sensing images.

SMART REMOTE SENSING IMAGE MOSAICKING

In terms of mosaicking multiple remote sensing images, the traditional idea is to mosaic them frame by frame, including image registration, radiometric normalization, and seamline detection. Within the last 10 years, multiframe joint methods have been proposed for seamline detection. Compared with frame-to-frame methods, multiframe joint methods show superiority by being independent of the processing sequence and not requiring intermediate treatment. The multiframe joint strategy should also be introduced into image registration and radiometric normalization. The accumulated errors from frame-to-frame methods will be alleviated and optimized. In other words, the multiframe joint strategy is smarter in terms of global restriction and adjustment.

As noted previously, the overlapping areas are the basis of mosaicking (radiometric normalization, seamline detection, and image blending). When the overlapping areas occupy a small part of the image, a satisfactory mosaicking result is very difficult to achieve. For better results, it is preferable to mosaic images with a low ratio of overlapping regions. Usually, remote sensing image mosaicking is preformed by variegating the images with geographical coordinates. Regarding remote sensing images without geographical information, a wise solution should be provided in the future.

Additionally, image-internal-information-based methods of seamline detection are often inefficient in complicated regions. Multiframe joint methods provide an available and smart approach with the aid of external data. In practical application software (e.g., Inpho OrthoVista), to obtain an ideal optimal seamline, human editing is usually needed. The fully automated optimal seamline should be detected by a smart strategy. In summary, smart remote sensing image mosaicking should pursue this direction.

CONCLUSIONS

In this article, we provided a comprehensive and quantitative summary of remote sensing image mosaicking in relation to the aspects of radiometric normalization, seamline detection, and image blending. Over the past few decades, many attempts have been made to improve the quality of image mosaicking. However, the process of achieving a perfect mosaic image still faces several challenges. Future research on remote sensing image mosaicking will use GAINS techniques. In other words, the application and concept of remote sensing image mosaicking should be *generalized*, the computation speed *accelerated*, the processing procedure *integrated*, and the processing strategy *smart*.

ACKNOWLEDGMENTS

The work was supported by the National Key R&D Program of China under grant 2017YFA0604402; the National Natural Science Foundation of China under grants 41701394 and 61671334; the Hubei Natural Science Foundation under grant 2017CFB189; the Open Research Fund of the Key Laboratory of Digital Mapping and Land Information Application Engineering under grant ZRZYBWD201903; and the Key Laboratory of Spatial Data Mining and Information Sharing, Fuzhou University, under grant 2018LSDMIS02.

AUTHOR INFORMATION

Xinghua Li (lixinghua5540@whu.edu.cn) received his B.S. degree in geographical information systems and Ph.D. degree in cartography and geographical information engineering from Wuhan University, China, in 2011 and 2016, respectively. He is currently with the School of Remote Sensing and Information Engineering, Wuhan University, as a distinguished associate researcher. His current research interests focus on multitemporal remote sensing analysis and application, remote sensing image processing, deep learning, and sparse representation. He has served as a reviewer for several journals, such as *IEEE Transactions on Geoscience and Remote Sensing*, *International Journal of Remote Sensing*, *IEEE Journal of Selected Topics in Applied Earth Observations and Remote Sensing*, and *Journal of Applied Remote Sensing*. He is a Member of the IEEE.

Ruitao Feng (ruitaofeng@whu.edu.cn) received her B.S. degree in geographic information systems from Hohai

University, Nanjing, China, in 2015. She is currently pursuing her Ph.D. degree with the School of Resource and Environment Sciences, Wuhan University, China. Her research interests include remote sensing images registration, geometric processing, and mosaicking.

Xiaobin Guan (guanxb@whu.edu.cn) received his B.S. and Ph.D. degrees in geographical information systems from the School of Resource and Environmental Sciences, Wuhan University, China, in 2013 and 2018, respectively and is currently a postdoctoral research assistant there. His research interests include the processing of multisource remote sensing images and its application in the terrestrial ecosystem and global change.

Huanfeng Shen (shenhf@whu.edu.cn) received his B.S. degree in surveying and mapping engineering and Ph.D. degree in photogrammetry and remote sensing from Wuhan University, China, in 2002 and 2007, respectively. In 2007, he joined the School of Resource and Environmental Sciences, Wuhan University, where he is currently a Luojia Distinguished Professor. He has authored more than 100 research papers and is currently a member of the editorial board of *Journal of Applied Remote Sensing*. He has been supported by several talent programs, such as the Youth Talent Support Program of China in 2015, the China National Science Fund for Excellent Young Scholars in 2014, and the New Century Excellent Talents by the Ministry of Education of China in 2011. His research interests include image quality improvement, remote sensing mapping and application, data fusion and assimilation, and regional and global environmental change. He is a Senior Member of the IEEE.

Liangpei Zhang (zlp62@whu.edu.cn) received his B.S. degree in physics from Hunan Normal University, Changsha, China, in 1982, M.S. degree in optics from the Xi'an Institute of Optics and Precision Mechanics, Chinese Academy of Sciences, China, in 1988, and Ph.D. degree in photogrammetry and remote sensing from Wuhan University, China, in 1998. He is currently the head of the Remote Sensing Division, State Key Laboratory of Information Engineering in Surveying, Mapping, and Remote Sensing, Wuhan University. He is also a Chang-Jiang Scholar Chair Professor appointed by the Ministry of Education of China. He is the founding chair of the IEEE GRSS Wuhan Chapter, a Fellow of the IEEE and the Institution of Engineering and Technology, and an executive member (Board of Governors) of the China National Committee of International Geosphere–Biosphere Program and the China Society of Image and Graphics.

REFERENCES

[1] M. Brown and D. G. Lowe, "Automatic panoramic image stitching using invariant features," *Int. J. Comput. Vis.*, vol. 74, no. 1, pp. 59–73, 2007. doi: 10.1007/s11263-006-0002-3.

[2] P. J. Burt and E. H. Adelson, "A multiresolution spline with application to image mosaics," *ACM Trans. Graph.*, vol. 2, no. 4, pp. 217–236, 1983. doi: 10.1145/245.247.

[3] X. Li, N. Hui, H. Shen, Y. Fu, and L. Zhang, "A robust mosaicking procedure for high spatial resolution remote sensing images," *ISPRS J. Photogrammetry Remote Sensing*, vol. 109, pp. 108–125, 2015. doi: 10.1016/j.isprsjprs.2015.09.009.

[4] D. V. Fedorov, L. M. G. Fonseca, C. Kenney, and B. S. Manjunath, "Automatic registration and mosaicking system for remotely sensed imagery," in *Proc. Int. Symp. Remote Sensing*, 2003, pp. 444–451.

[5] G. De Grandi, J.-P. Malingreau, and M. Leysen, "The ERS-1 Central Africa Mosaic: A new perspective in radar remote sensing for the global monitoring of vegetation," *IEEE Trans. Geosci. Remote Sens.*, vol. 37, no. 3, pp. 1730–1746, 1999. doi: 10.1109/36.763296.

[6] D. Turner, A. Lucieer, and C. Watson, "An automated technique for generating georectified mosaics from ultra-high resolution unmanned aerial vehicle (UAV) imagery, based on structure from motion (SfM) point clouds," *Remote Sensing*, vol. 4, no. 5, pp. 1392–1410, 2012. doi: 10.3390/rs4051392.

[7] C. J. Tucker, D. M. Grant, and J. D. Dykstra, "NASA's global orthorectified Landsat data set," *Photogrammetric Eng. Remote Sensing*, vol. 70, no. 3, pp. 313–322, 2004. doi: 10.14358/PERS.70.3.313.

[8] R. H. Merson, "An AVHRR mosaic image of Antarctica," *Int. J. Remote Sens.*, vol. 10, no. 4–5, pp. 669–674, 1989. doi: 10.1080/01431168908903908.

[9] A. Rosenqvist et al., "The Global Rain Forest Mapping project–A review," *Int. J. Remote Sens.*, vol. 21, no. 6–7, pp. 1375–1387, 2000. doi: 10.1080/014311600210227.

[10] G. De Grandi, P. Mayaux, Y. Rauste, A. Rosenqvist, M. Simard, and S. S. Saatchi, "The Global Rain Forest Mapping Project JERS-1 radar mosaic of tropical Africa: Development and product characterization aspects," *IEEE Trans. Geosci. Remote Sens.*, vol. 38, no. 5, pp. 2218–2233, 2000. doi: 10.1109/36.868880.

[11] R. Feng, Q. Du, X. Li, and H. Shen, "Robust registration for remote sensing images by combining and localizing feature- and area-based methods," *ISPRS J. Photogrammetry Remote Sensing*, vol. 151, pp. 15–26, 2019. doi: 10.1016/j.isprsjprs.2019.03.002.

[12] Q. Du, N. Raksuntorn, A. Orduyilmaz, and L. M. Bruce, "Automatic registration and mosaicking for airborne multispectral image sequences," *Photogrammetric Eng. Remote Sensing*, vol. 74, no. 2, pp. 169–181, 2008. doi: 10.14358/PERS.74.2.169.

[13] C. Zhong, Q. Xu, and B. Li, "Relative radiometric normalization for multitemporal remote sensing images by hierarchical regression," *IEEE Geosci. Remote Sens. Lett.*, vol. 13, no. 2, pp. 217–221, 2016. doi: 10.1109/LGRS.2015.2506643.

[14] W. Zhang, B. Guo, M. Li, X. Liao, and W. Li, "Improved seamline searching algorithm for UAV image mosaic with optical flow," *Sensors*, vol. 18, no. 4, pp. 1214–1228, 2018. doi: 10.3390/s18041214.

[15] L. Li, J. Yao, R. Xie, and J. Li, "Edge-Enhanced optimal seamline detection for orthoimage mosaicking," *IEEE Geosci. Remote Sens. Lett.*, vol. 15, no. 5, pp. 764–768, 2018. doi: 10.1109/LGRS.2018.2805324.

[16] R. T. Whitaker, "A level-set approach to image blending," *IEEE Trans. Image Process.*, vol. 9, no. 11, pp. 1849–1861, 2000. doi: 10.1109/83.877208.

[17] D.-H. Kim, Y.-I. Yoon, and J.-S. Choi, "An efficient method to build panoramic image mosaics," *Pattern Recognit. Lett.*, vol. 24, no. 14, pp. 2421–2429, 2003. doi: 10.1016/S0167-8655(03)00071-0.

[18] Z. Hua, Y. Li, and J. Li, "Image stitch algorithm based on SIFT and MVSC," in *Proc. 2010 7th Int. Conf. Fuzzy Systems and Knowledge Discovery*, pp. 2628–2632.

[19] T. Suzuki, Y. Amano, and T. Hashizume, "Vision based localization of a small UAV for generating a large mosaic image," in *Proc. SICE Annu. Conf. 2010*, pp. 2960–2964.

[20] J. Shi, J. Wang, and Y. Xu, "Use of GPS/INS observations for efficient matching of UAV images," in *Proc. Int. Global Navigation Satellite Systems Society Symp.*, 2011.

[21] B. Zitová and J. Flusser, "Image registration methods: A survey," *Image Vis. Comput.*, vol. 21, no. 11, pp. 977–1000, 2003. doi: 10.1016/S0262-8856(03)00137-9.

[22] S. Dawn, V. Saxena, and B. Sharma, "Remote sensing image registration techniques: A survey," in *Proc. Int. Conf. Image and Signal Processing*, 2010, pp. 103–112.

[23] S. S. Bisht, B. Gupta, and P. Rahi, "Image registration concept and techniques: A review," *J. Eng. Res. Appl.*, vol. 4, no. 4, pp. 30–35, 2014.

[24] C. P. Dalmiya and V. S. Dharun, "A survey of registration techniques in remote sensing images," *Indian J. Sci. Technol.*, vol. 8, no. 26, pp. 1–5, 2015. doi: 10.17485/ijst/2015/v8i26/81048.

[25] A. Mills and G. Dudek, "Image stitching with dynamic elements," *Image Vis. Comput.*, vol. 27, no. 10, pp. 1593–1602, 2009. doi: 10.1016/j.imavis.2009.03.004.

[26] R. Cresson and N. Saint-Geours, "Natural color satellite image mosaicking using quadratic programming in decorrelated color space," *IEEE J. Sel. Topics Appl. Earth Observ. Remote Ses.*, vol. 8, no. 8, pp. 4151–4162, 2015. doi: 10.1109/JSTARS.2015.2449233.

[27] W. Xu and J. Mulligan, "Performance evaluation of color correction approaches for automatic multi-view image and video stitching," in *Proc. 2010 IEEE Computer Society Conf. Computer Vision and Pattern Recognition*, pp. 263–270.

[28] C. Cariou and K. Chehdi, "Fully automated mosaicking of pushbroom aerial imagery," in *Proc. 2008 IEEE Int. Conf. Acoustics, Speech and Signal Processing*, pp. 1105–1108.

[29] X. Han, H. Cao, Z. Yuan, H. Zhao, and L. Yan, "An approach of color image mosaicking based on color vision characteristics," in *Proc. 2009 3rd Int. Conf. Genetic and Evolutionary Computing*, pp. 343–346.

[30] L. Zhang, C. Wu, and B. Du, "Automatic radiometric normalization for multitemporal remote sensing imagery with iterative slow feature analysis," *IEEE Trans. Geosci. Remote Sens.*, vol. 52, no. 10, pp. 6141–6155, 2014. doi: 10.1109/TGRS.2013.2295263.

[31] C. Chen, Z. Chen, M. Li, Y. Liu, L. Cheng, and Y. Ren, "Parallel relative radiometric normalisation for remote sensing image mosaics," *Comput. Geosci.*, vol. 73, pp. 28–36, 2014. doi: 10.1016/j.cageo.2014.08.007.

[32] M. A. Syariz, B.-Y. Lin, L. G. Denaro, L. M. Jaelani, M.-V. Nguyen, and C.-H. Lin, "Spectral-consistent relative radiometric normalization for multitemporal Landsat 8 imagery," *ISPRS J. Photogrammetry Remote Sensing*, vol. 147, pp. 56–64, 2019. doi: 10.1016/j.isprsjprs.2018.11.007.

[33] Y. Du, J. Cihlar, J. Beaubien, and R. Latifovic, "Radiometric normalization, compositing, and quality control for satellite high resolution image mosaics over large areas," *IEEE Trans. Geosci. Remote Sens.*, vol. 39, no. 3, pp. 623–634, 2001. doi: 10.1109/36.911119.

[34] M. Zhang and N. D. Georganas, "Fast color correction using principal regions mapping in different color spaces," *Real-Time Imaging*, vol. 10, no. 1, pp. 23–30, 2004. doi: 10.1016/j.rti.2003.11.001.

[35] A. Litvinov and Y. Y. Schechner, "Radiometric framework for image mosaicking," *J. Opt. Soc. Amer. A, Opt. Image Sci.*, vol. 22, no. 5, pp. 839–848, 2005. doi: 10.1364/JOSAA.22.000839.

[36] M. J. Canty and A. A. Nielsen, "Automatic radiometric normalization of multitemporal satellite imagery with the iteratively re-weighted MAD transformation," *Remote Sens. Environ.*, vol. 112, no. 3, pp. 1025–1036, 2008. doi: 10.1016/j.rse.2007.07.013.

[37] G. Y. Tian, D. Gledhill, and D. Taylor, "Comprehensive interest points based imaging mosaic," *Pattern Recognit. Lett.*, vol. 24, no. 9–10, pp. 1171–1179, 2003. doi: 10.1016/S0167-8655(02)00287-8.

[38] B. V. Funt and B. C. Lewis, "Diagonal versus affine transformations for color correction," *J. Opt. Soc. Amer. A, Opt. Image Sci.*, vol. 17, no. 11, pp. 2108–2112, 2000. doi: 10.1364/JOSAA.17.002108.

[39] G. Y. Tian, D. Gledhill, D. Taylor, and D. Clarke, "Colour correction for panoramic imaging," in *Proc. 6th Int. Conf. Information Visualisation*, 2002, pp. 483–488.

[40] Z. Zhang, Z. Li, J. Zhang, and L. Zheng, "Use of discrete chromatic space to tune the image tone in a color image mosaic," in *Proc. 3rd Int. Symp. Multispectral Image Processing and Pattern Recognition*, 2003, pp. 16–21.

[41] L. Li, J. Yao, R. Xie, M. Xia, and W. Zhang, "A unified framework for street-view panorama stitching," *Sensors*, vol. 17, no. 1, pp. 1–27, 2017. doi: 10.3390/s17010001.

[42] X. J. Yang and C. P. Lo, "Relative radiometric normalization performance for change detection from multi-date satellite images," *Photogrammetric Eng. Remote Sensing*, vol. 66, no. 8, pp. 967–980, 2000.

[43] F. L. Gadallah, F. Csillag, and E. J. M. Smith, "Destriping multisensor imagery with moment matching," *Int. J. Remote Sens.*, vol. 21, no. 12, pp. 2505–2511, 2000. doi: 10.1080/01431160050030592.

[44] J. Liu et al., "Illumination and contrast balancing for remote sensing images," *Remote Sensing*, vol. 6, no. 2, pp. 1102–1123, 2014. doi: 10.3390/rs6021102.

[45] M. W. Sun and J. Q. Zhang, "Dodging research for digital aerial images," in *Proc. 21st Int. Society for Photogrammetry and Remote Sensing Congr.*, 2008, pp. 349–354.

[46] R. Xie, M. Xia, J. Yao, and L. Li, "Guided color consistency optimization for image mosaicking," *ISPRS J. Photogrammetry*

Remote Sensing, vol. 135, pp. 43–59, 2018. doi: 10.1016/j.isprsjprs.2017.11.012.

[47] J. Jia, J. Sun, C.-K. Tang, and H.-Y. Shum, "Bayesian correction of image intensity with spatial consideration," in *Proc. 8th European Conf. Computer Vision*, 2004, pp. 342–354.

[48] S. J. Kim and M. Pollefeys, "Robust radiometric calibration and vignetting correction," *IEEE Trans. Pattern Anal. Mach. Intell.*, vol. 30, no. 4, pp. 562–576, 2008. doi: 10.1109/TPAMI.2007.70732.

[49] K. Yamamoto and R. Oi, "Color correction for multi-view video using energy minimization of view networks," *Int. J. Automation Computing*, vol. 5, no. 3, pp. 234–245, 2008. doi: 10.1007/s11633-008-0234-5.

[50] E. Reinhard, M. Adhikhmin, B. Gooch, and P. Shirley, "Color transfer between images," *IEEE Comput. Graph. Appl. Mag.*, vol. 21, no. 5, pp. 34–41, 2001. doi: 10.1109/38.946629.

[51] L. Yu, Y. Zhang, M. Sun, and X. Zhu, "Colour balancing of satellite imagery based on a colour reference library," *Int. J. Remote Sens.*, vol. 37, no. 24, pp. 5763–5785, 2016. doi: 10.1080/01431161.2016.1249306.

[52] Y.-W. Tai, J. Jia, and C.-K. Tang, "Local color transfer via probabilistic segmentation by expectation-maximization," in *Proc. 2005 IEEE Computer Society Conf. Computer Vision and Pattern Recognition*, pp. 747–754.

[53] Y. Xiang, B. Zou, and H. Li, "Selective color transfer with multi-source images," *Pattern Recognit. Lett.*, vol. 30, no. 7, pp. 682–689, 2009. doi: 10.1016/j.patrec.2009.01.004.

[54] M. Oliveira, A. D. Sappa, and V. Santos, "A probabilistic approach for color correction in image mosaicking applications," *IEEE Trans. Image Process.*, vol. 24, no. 2, pp. 508–523, 2015. doi: 10.1109/TIP.2014.2375642.

[55] J. Li, Q. Hu, and M. Ai, "Optimal illumination and color consistency for optical remote-sensing image mosaicking," *IEEE Geosci. Remote Sens. Lett.*, vol. 14, no. 11, pp. 1943–1947, 2017. doi: 10.1109/LGRS.2017.2743209.

[56] J. Jia and C.-K. Tang, "Image registration with global and local luminance alignment," in *Proc. 9th IEEE Int. Conf. Computer Vision*, 2003, pp. 156–163.

[57] J. Jia and C.-K. Tang, "Tensor voting for image correction by global and local intensity alignment," *IEEE Trans. Pattern Anal. Mach. Intell.*, vol. 27, no. 1, pp. 36–50, 2005. doi: 10.1109/TPAMI.2005.20.

[58] J. Pan, M. Wang, D. Li, and J. Li, "A network-based radiometric equalization approach for digital aerial orthoimages," *IEEE Geosci. Remote Sens. Lett.*, vol. 7, no. 2, pp. 401–405, 2010. doi: 10.1109/LGRS.2009.2037442.

[59] L. Yu, Y. Zhang, M. Sun, X. Zhou, and C. Liu, "An auto-adapting global-to-local color balancing method for optical imagery mosaic," *ISPRS J. Photogrammetry Remote Sensing*, vol. 132, pp. 1–19, 2017. doi: 10.1016/j.isprsjprs.2017.08.002.

[60] M.-L. Duplaquet, "Building large image mosaics with invisible seam lines," in *Proc. Visual Information Processing and Communication*, 1998, pp. 369–377.

[61] E. Zagrouba, W. Barhoumi, and S. Amri, "An efficient image-mosaicing method based on multifeature matching," *Mach. Vis. Appl.*, vol. 20, no. 3, pp. 139–162, 2009. doi: 10.1007/s00138-007-0114-y.

[62] E. Fernandez, R. Garfinkel, and R. Arbiol, "Mosaicking of aerial photographic maps via seams defined by bottleneck shortest paths," *Oper. Res.*, vol. 46, no. 3, pp. 293–304, 1998. doi: 10.1287/opre.46.3.293.

[63] M. Kass, A. Witkin, and D. Terzopoulos, "Snakes: Active contour models," *Int. J. Comput. Vis.*, vol. 1, no. 4, pp. 321–331, 1988. doi: 10.1007/BF00133570.

[64] E. W. Dijkstra, "A note on two problems in connexion with graphs," *Numerische Mathematik*, vol. 1, no. 1, pp. 269–271, 1959. doi: 10.1007/BF01386390.

[65] H. Agrawal and J. R. Horgan, "Dynamic program slicing," in *Proc. ACM SIGPLAN 1990 Conf. Programming Language Design and Implementation*, pp. 246–256.

[66] D. M. Greig, B. T. Porteous, and A. H. Seheult, "Exact maximum a posteriori estimation for binary images," *J. Roy. Statistical Soc.: Series B (Methodological)*, vol. 51, no. 2, pp. 271–279, 1989. doi: 10.1111/j.2517-6161.1989.tb01764.x.

[67] E. Fernández and R. Martí, "GRASP for seam drawing in mosaicking of aerial photographic maps," *J. Heuristics*, vol. 5, no. 2, pp. 181–197, 1999. doi: 10.1023/A:1009633811636.

[68] L. Wang, H. Ai, and L. Zhang, "Automated seamline detection in orthophoto mosaicking using improved snakes," in *Proc. 2010 2nd Int. Conf. Information Engineering and Computer Science*, pp. 1–4.

[69] M. Kerschner, "Seamline detection in colour orthoimage mosaicking by use of twin snakes," *ISPRS J. Photogrammetry Remote Sensing*, vol. 56, no. 1, pp. 53–64, 2001. doi: 10.1016/S0924-2716(01)00033-8.

[70] M. Kerschner, "Twin snakes for determining seam lines in orthoimage mosaicking," in *Proc. 19th Int. Society for Photogrammetry and Remote Sensing Congr.*, 2000, pp. 454–461.

[71] J. Chon and H. Kim, "Determination of the optimal seam-lines in image mosaicking with the dynamic programming (DP) on the converted cost space," in *Proc. Int. Conf. Artificial Intelligence and Soft Computing*, 2006, pp. 750–757.

[72] J. Davis, "Mosaics of scenes with moving objects," in *Proc. 1998 IEEE Computer Society Conf. Computer Vision and Pattern Recognition*, pp. 354–360.

[73] Y. Afek and A. Brand, "Mosaicking of orthorectified aerial images," *Photogrammetric Eng. Remote Sensing*, vol. 64, no. 2, pp. 115–124, 1998.

[74] J. Pan, Q. Zhou, and M. Wang, "Seamline determination based on segmentation for urban image mosaicking," *IEEE Geosci. Remote Sens. Lett.*, vol. 11, no. 8, pp. 1335–1339, 2014. doi: 10.1109/LGRS.2013.2293197.

[75] S. Pang, M. Sun, X. Hu, and Z. Zhang, "SGM-based seamline determination for urban orthophoto mosaicking," *ISPRS J. Photogrammetry Remote Sensing*, vol. 112, pp. 1–12, 2016. doi: 10.1016/j.isprsjprs.2015.11.007.

[76] J. Pan, M. Wang, J. Li, S. Yuan, and F. Hu, "Region change rate-driven seamline determination method," *ISPRS J. Photogrammetry Remote Sensing*, vol. 105, pp. 141–154, 2015. doi: 10.1016/j.isprsjprs.2015.04.004.

[77] M. Wang, S. Yuan, J. Pan, L. Fang, Q. Zhou, and G. Yang, "Seamline determination for high resolution orthoimage mosaicking using watershed segmentation," *Photogrammetric Eng.*

Remote Sensing, vol. 82, no. 2, pp. 121–133, 2016. doi: 10.14358/PERS.82.2.121.

[78] P. Soille, "Morphological image compositing," *IEEE Trans. Pattern Anal. Mach. Intell.*, vol. 28, no. 5, pp. 673–683, 2006. doi: 10.1109/TPAMI.2006.99.

[79] H. Wen and J. Zhou, "An improved algorithm for image mosaic," in *Proc. 2008 Int. Symp. Information Science and Engineering*, pp. 497–500.

[80] J. Chon, H. Kim, and C.-S. Lin, "Seam-line determination for image mosaicking: A technique minimizing the maximum local mismatch and the global cost," *ISPRS J. Photogrammetry Remote Sensing*, vol. 65, no. 1, pp. 86–92, 2010. doi: 10.1016/j.isprsjprs.2009.09.001.

[81] C. Xing, J. Wang, and Y. Xu, "An optimal seamline based mosaic method for UAV sequence images," in *Proc. Int. Conf. Civil and Environmental Engineering*, 2010.

[82] N. Gracias, M. Mahoor, S. Negahdaripour, and A. Gleason, "Fast image blending using watersheds and graph cuts," *Image Vis. Comput.*, vol. 27, no. 5, pp. 597–607, 2009. doi: 10.1016/j.imavis.2008.04.014.

[83] C. Allene, J.-P. Pons, and R. Keriven, "Seamless image-based texture atlases using multi-band blending," in *Proc. 2008 19th Int. Conf. Pattern Recognition*, pp. 1–4.

[84] V. Kwatra, A. Schödl, I. Essa, G. Turk, and A. Bobick, "Graphcut textures: Image and video synthesis using graph cuts," *ACM Trans. Graph.*, vol. 22, no. 3, pp. 277–286, 2003. doi: 10.1145/882262.882264.

[85] A. Agarwala et al., "Interactive digital photomontage," *ACM Trans. Graph.*, vol. 23, no. 3, pp. 294–302, 2004. doi: 10.1145/1015706.1015718.

[86] Z. Qu, T. Wang, S. An, and L. Liu, "Image seamless stitching and straightening based on the image block," *IET Image Process.*, vol. 12, no. 8, pp. 1361–1369, 2018. doi: 10.1049/iet-ipr.2017.1064.

[87] A. Levin, A. Zomet, S. Peleg, and Y. Weiss, "Seamless image stitching in the gradient domain," in *Proc. European Conf. Computer Vision*, 2004, pp. 377–389.

[88] A. Zomet, A. Levin, S. Peleg, and Y. Weiss, "Seamless image stitching by minimizing false edges," *IEEE Trans. Image Process.*, vol. 15, no. 4, pp. 969–977, 2006. doi: 10.1109/TIP.2005.863958.

[89] Y. Yang, Y. Gao, H. Li, and Y. Han, "An algorithm for remote sensing image mosaic based on valid area," in *Proc. 2011 Int. Symp. Image and Data Fusion*, pp. 1–4.

[90] C.-M. Huang, S.-W. Lin, and J.-H. Chen, "Efficient image stitching of continuous image sequence with image and seam selections," *IEEE Sensors J.*, vol. 15, no. 10, pp. 5910–5918, 2015. doi: 10.1109/JSEN.2015.2449879.

[91] T. L. Nguyen, Y. Byun, D. Han, and J. Huh, "Efficient seamline determination for UAV image mosaicking using edge detection," *Remote Sensing Lett.*, vol. 9, no. 8, pp. 763–769, 2018. doi: 10.1080/2150704X.2018.1475772.

[92] S. Laaroussi, A. Baataoui, A. Halli, and S. Khalid, "A dynamic mosaicking method based on histogram equalization for an improved seamline," *Procedia Comput. Sci.*, vol. 127, pp. 344–352, 2018. doi: 10.1016/j.procs.2018.01.131.

[93] R. Xandri, F. Pérez-Aragüés, V. Palà, and R. Arbiol, "Automatic generation of seamless mosaics over extensive areas from high resolution imagery," in *Proc. 9th World Multi-Conf. Systemics, Cybernetics and Informatics*, 2005, pp. 1–6.

[94] S. Hsu, H. S. Sawhney, and R. Kumar, "Automated mosaics via topology inference," *IEEE Comput. Graph. Appl. Mag.*, vol. 22, no. 2, pp. 44–54, 2002. doi: 10.1109/38.988746.

[95] J. Pan, M. Wang, D. Li, and J. Li, "Automatic generation of seamline network using area Voronoi diagrams with overlap," *IEEE Trans. Geosci. Remote Sens.*, vol. 47, no. 6, pp. 1737–1744, 2009.

[96] J. Pan, M. Wang, D. Ma, Q. Zhou, and J. Li, "Seamline network refinement based on area Voronoi diagrams with overlap," *IEEE Trans. Geosci. Remote Sens.*, vol. 52, no. 3, pp. 1658–1666, 2014.

[97] M. Song, Z. Ji, S. Huang, and J. Fu, "Mosaicking UAV orthoimages using bounded Voronoi diagrams and watersheds," *Int. J. Remote Sens.*, vol. 39, no. 15–16, pp. 4960–4979, 2018. doi: 10.1080/01431161.2017.1350309.

[98] L. Li, J. Yao, X. Lu, J. Tu, and J. Shan, "Optimal seamline detection for multiple image mosaicking via graph cuts," *ISPRS J. Photogrammetry Remote Sensing*, vol. 113, pp. 1–16, 2016. doi: 10.1016/j.isprsjprs.2015.12.007.

[99] S. Mills and P. McLeod, "Global seamline networks for orthomosaic generation via local search," *ISPRS J. Photogrammetry Remote Sensing*, vol. 75, pp. 101–111, 2013. doi: 10.1016/j.isprsjprs.2012.11.003.

[100] J. Pan, Z. Fang, S. Chen, H. Ge, F. Hu, and M. Wang, "An improved seeded region growing-based seamline network generation method," *Remote Sens.*, vol. 10, no. 7, pp. 1065–1084, 2018. doi: 10.3390/rs10071065.

[101] H.-C. Ma and J. Sun, "Intelligent optimization of seam-line finding for orthophoto mosaicking with LiDAR point clouds," *J. Zhejiang University Sci. C*, vol. 12, no. 5, pp. 417–429, 2011. doi: 10.1631/jzus.C1000235.

[102] D. Wang, Y. Wan, J. Xiao, X. Lai, W. Huang, and J. Xu, "Aerial image mosaicking with the aid of vector roads," *Photogrammetric Eng. Remote Sensing*, vol. 78, no. 11, pp. 1141–1150, 2012.

[103] Y. Wan, D. Wang, J. Xiao, X. Lai, and J. Xu, "Automatic determination of seamlines for aerial image mosaicking based on vector roads alone," *ISPRS J. Photogrammetry Remote Sensing*, vol. 76, pp. 1–10, 2013. doi: 10.1016/j.isprsjprs.2012.11.002.

[104] R. W. Floyd, "Algorithm 97: Shortest path," *Commun. ACM*, vol. 5, no. 6, pp. 345, 1962. doi: 10.1145/367766.368168.

[105] L. Yu, E.-J. Holden, M. C. Dentith, and H. Zhang, "Towards the automatic selection of optimal seam line locations when merging optical remote-sensing images," *Int. J. Remote Sens.*, vol. 33, no. 4, pp. 1000–1014, 2012. doi: 10.1080/01431161.2010.545083.

[106] E. Niebur, "Saliency map," *Scholarpedia*, vol. 2, no. 8, pp. 2675, 2007. doi: 10.4249/scholarpedia.2675.

[107] J. Pan, S. Yuan, J. Li, and B. Wu, "Seamline optimization based on ground objects classes for orthoimage mosaicking," *Remote Sensing Lett.*, vol. 8, no. 3, pp. 280–289, 2017. doi: 10.1080/2150704X.2016.1264023.

[108] Q. Chen, M. Sun, X. Hu, and Z. Zhang, "Automatic seamline network generation for urban orthophoto mosaicking with the

use of a digital surface model," *Remote Sens.*, vol. 6, no. 12, pp. 12,334–12,359, 2014. doi: 10.3390/rs61212334.

[109] M. Zheng, X. Xiong, and J. Zhu, "Automatic seam-line determination for orthoimage mosaics using edge-tracking based on a DSM," *Remote Sensing Lett.*, vol. 8, no. 10, pp. 977–986, 2017. doi: 10.1080/2150704X.2017.1343509.

[110] M. Zheng, S. Zhou, X. Xiong, and J. Zhu, "A novel orthoimage mosaic method using the weighted A* algorithm for UAV imagery," *Comput. Geosci.*, vol. 109, pp. 238–246, 2017. doi: 10.1016/j.cageo.2017.08.004.

[111] M. Al-Durgham, M. Downey, S. Gehrke, and B. T. Beshah, "A framework for an automatic seamline engine," in *Proc. 23rd Int. Society for Photogrammetry and Remote Sensing Congr.*, 2016, pp. 275–280. doi: 10.5194/isprs-archives-XLI-B1-275-2016.

[112] Y. Zhang, M. Zhang, S. Du, Z. Zou, and C. Fan, "Seamline optimisation for urban aerial ortho-image mosaicking using graph cuts," *Photogrammetric Rec.*, vol. 33, no. 161, pp. 131–147, 2018. doi: 10.1111/phor.12232.

[113] S. Peleg, "Elimination of seams from photomosaics," *Comput. Graph. Image Process.*, vol. 16, no. 1, pp. 90–94, 1981. doi: 10.1016/0146-664X(81)90094-0.

[114] S. Zhu and Z. Qian, "The seam-line removal under mosaicking of remotely sensed images," *J. Remote Sens.*, vol. 6, no. 3, pp. 183–187, 2002.

[115] W. Liu, J. Shen, and W. Chen, "Image mosaic technology based on overlapped area linear transition method," in *Proc. 2009 2nd Int. Congr. Image and Signal Processing*, pp. 1–3.

[116] D. L. Milgram, "Computer methods for creating photomosaics," *IEEE Trans. Comput.*, vol. C-24, no. 11, pp. 1113–1119, 1975. doi: 10.1109/T-C.1975.224142.

[117] P. Pérez, M. Gangnet, and A. Blake, "Poisson image editing," *ACM Trans. Graph.*, vol. 22, no. 3, pp. 313–318, 2003. doi: 10.1145/882262.882269.

[118] J. Jia and C.-K. Tang, "Image stitching using structure deformation," *IEEE Trans. Pattern Anal. Mach. Intell.*, vol. 30, no. 4, pp. 617–631, 2008. doi: 10.1109/TPAMI.2007.70729.

[119] F. Yang, L. Wei, Z. Zhang, and H. Tang, "Image mosaic based on phase correlation and Harris operator," *J. Comput. Inf. Syst.*, vol. 8, no. 6, pp. 2647–2655, 2012.

[120] M. Uyttendaele, A. Eden, and R. Skeliski, "Eliminating ghosting and exposure artifacts in image mosaics," in *Proc. 2001 IEEE Computer Society Conf. Computer Vision and Pattern Recognition*, pp. 509–516.

[121] C. C. Dos Santos, S. A. Stoeter, P. E. Rybski, and N. P. Papanikolopoulos, "Mosaicking images [panoramic imaging]," *IEEE Robot. Autom. Mag.*, vol. 11, no. 4, pp. 62–68, 2004. doi: 10.1109/MRA.2004.1371610.

[122] J. Pan, M. Wang, X. Cao, S. Chen, and F. Hu, "A multi-resolution blending considering changed regions for orthoimage mosaicking," *Remote Sens.*, vol. 8, no. 10, pp. 842–861, 2016. doi: 10.3390/rs8100842.

[123] H.-C. Shao, W.-L. Hwang, and Y.-C. Chen, "Optimal multiresolution blending of confocal microscope images," *IEEE Trans. Biomed. Eng.*, vol. 59, no. 2, pp. 531–541, 2012. doi: 10.1109/TBME.2011.2175446.

[124] V. Rankov, R. J. Locke, R. J. Edens, P. R. Barber, and B. Vojnovic, "An algorithm for image stitching and blending," in *Proc. SPIE 5701, Three-Dimensional and Multidimensional Microscopy: Image Acquisition and Processing XII*, 2005, pp. 190–199.

[125] D. Patidar and A. Jain, "Automatic image mosaicing: An approach based on FFT," *Int. J. Scientific Eng. Technol.*, vol. 1, no. 1, pp. 1–4, 2011.

[126] M.-S. Su, W.-L. Hwang, and K.-Y. Cheng, "Variational calculus approach to multiresolution image mosaic," in *Proc. 2001 Int. Conf. Image Processing*, pp. 245–248.

[127] W. Zhao, "Flexible image blending for image mosaicing with reduced artifacts," *Int. J. Pattern Recognition Artificial Intell.*, vol. 20, no. 4, pp. 609–628, 2006. doi: 10.1142/S0218001406004806.

[128] M.-S. Su, W.-L. Hwang, and K.-Y. Cheng, "Analysis on multiresolution mosaic images," *IEEE Trans. Image Process.*, vol. 13, no. 7, pp. 952–959, 2004. doi: 10.1109/TIP.2004.828416.

[129] W. Wang and M. K. Ng, "A variational method for multiple-image blending," *IEEE Trans. Image Process.*, vol. 21, no. 4, pp. 1809–1822, 2012. doi: 10.1109/TIP.2011.2176952.

[130] H. Nicolas, "New methods for dynamic mosaicking," *IEEE Trans. Image Process.*, vol. 10, no. 8, pp. 1239–1251, 2001. doi: 10.1109/83.935039.

[131] H. Shen et al., "Missing information reconstruction of remote sensing data: A technical review," *IEEE Geosci. Remote Sens. Mag.*, vol. 3, no. 3, pp. 61–85, 2015. doi: 10.1109/MGRS.2015.2441912.

[132] X. Li, H. Shen, L. Zhang, H. Zhang, Q. Yuan, and G. Yang, "Recovering quantitative remote sensing products contaminated by thick clouds and shadows using multitemporal dictionary learning," *IEEE Trans. Geosci. Remote Sens.*, vol. 52, no. 11, pp. 7086–7098, 2014. doi: 10.1109/TGRS.2014.2307354.

[133] X. Li, H. Shen, H. Li, and L. Zhang, "Patch matching-based multitemporal group sparse representation for the missing information reconstruction of remote-sensing images," *IEEE J. Select. Topics Appl. Earth Observ. Remote Ses.*, vol. 9, no. 8, pp. 3629–3641, 2016. doi: 10.1109/JSTARS.2016.2533547.

[134] X. Li, L. Wang, Q. Cheng, P. Wu, W. Gan, and L. Fang, "Cloud removal in remote sensing images using nonnegative matrix factorization and error correction," *ISPRS J. Photogrammetry Remote Sens.*, vol. 148, pp. 103–113, 2019. doi: 10.1016/j.isprsjprs.2018.12.013.

[135] L. Chen, Y. Ma, P. Liu, J. Wei, W. Jie, and J. He, "A review of parallel computing for large-scale remote sensing image mosaicking," *Cluster Computing*, vol. 18, no. 2, pp. 517–529, 2015. doi: 10.1007/s10586-015-0422-3.

[136] Y. Ma et al., "Remote sensing big data computing: Challenges and opportunities," *Future Gener. Comput. Syst.*, vol. 51, pp. 47–60, 2015. doi: 10.1016/j.future.2014.10.029.

[137] C. A. Lee, S. D. Gasster, A. Plaza, C.-I. Chang, and B. Huang, "Recent developments in high performance computing for remote sensing: A review," *IEEE J. Select. Topics Appl. Earth Observ. Remote Ses.*, vol. 4, no. 3, pp. 508–527, 2011. doi: 10.1109/JSTARS.2011.2162643.

[138] H. Zhang, Z. Shi, K. Pang, Y. Jia, and T. Luo, "A real-time image stitching method based on memory space conversion," in *Proc. 2015 8th Int. Congr. Image and Signal Processing (CISP)*, pp. 856–860.

GRS